Influence of TiO_2-based photocatalytic coating road on traffic-related NO_x pollutants in urban street canyon by CFD modeling

*Xiaomin Xie*1, Chenrui Hao1, Yue Huang2, Zhen Huang1,*

1 Key Laboratory for Power machinery and Engineering of M. O. E., Shanghai Jiao Tong University, No. 800, Dongchuan Road, 200240 Shanghai, P R China

2 Institute for Transport Studies, University of Leeds, 34-40 University Road, Leeds, LS2 9JT, UK

ABSTRACT

The use of titanium dioxide (TiO_2) photocatalytic nanoparticles as road coating to trap and decompose air pollutants provides a promising technology to mitigate the harmful effects of vehicle emissions. However, there are few studies on computational fluid dynamics (CFD) simulations of the effect of NOx photocatalytic oxidation in street canyon with TiO_2 nanoparticles as pavement coating. This study developed a CFD model with photocatalytic oxidation (PCO) reaction implemented for numerical simulation of NO_x abatement in an urban street canyon with TiO_2 coating, considering the effects of relative humidity (*RH*) (10–90%) and irradiance (10–40 $W \cdot m^{-2}$). Results show that TiO_2 coating road can effectively reduce nitrogen oxide (NO_x) concentration in the street canyon. The average nitric oxide (NO) and nitrogen dioxide (NO_2) concentrations in street canyon with TiO_2 coating road were reduced by 3.70% and 4.31%, respectively, comparing with street canyon without TiO_2 coating. The irradiance

and relative humidity had great effect on PCO reaction in street canyon with TiO_2 coating road. When the irradiance increased from $10 W \cdot m^{-2}$ to $40 W \cdot m^{-2}$, average NO conversion rose from 1.35% to 3.70%, and average NO_2 conversion rose from 2.43% to 4.31%. The average conversion of NO and NO_2 decreased from 5.11% to 2.54% and from 5.60% to 3.25%, respectively, when the relative humidity varied from 10% to 90%. Results are useful to transport planners and road engineers who need to reduce NOx concentrations in urban streets travelled by fossil fuel-powered vehicles. Method of the study can be considered by future research faced with different pavement construction and traffic environment.

Keywords: Street canyon; TiO_2 coating road; NO_x concentration; photocatalytic oxidation (PCO); computational fluid dynamics (CFD) simulation

1. Introduction

The total NO_x emissions were 12.59 Mt in China in 2017 (National Bureau of Statistics of China, 2019). Vehicle exhaust is a major contributor to NO_x emissions in cities with the rapidly growing automobile industry and urbanization. These activities yielded an increase of 1.4 Mt NOx in 2017 compared with the 2010 levels, while pollution control measures have yielded reductions of 1.3 Mt NO_x (Zheng et al., 2018). In 2017, NO_x emissions from vehicles were estimated to be 5.74 Mt (National Ministry of Ecology and Environment of China, 2018), accounting for 45.6% of the total NO_x

42 emissions in China. NO_x cause a wide range of environmental issues, such as the
43 formation of tropospheric ozone and urban smog through photochemical reactions with
44 hydrocarbons. Furthermore, NO_x can cause acute respiratory tract infections and
45 cardiovascular diseases (Notario et al., 2012). Road pavement, in initial and direct
46 contact with tailpipe emissions, provides an opportunity to retain and convert the
47 pollutants to less harmful substances. Photocatalytic oxidation (PCO) is found effective
48 in reducing air pollution caused by NOx. PCO using TiO_2 has drawn public attention
49 for air quality reasons with their advantages of high oxidation efficiency, innocuity and
50 low cost (Jiang et al., 2019).

51 Photocatalytic concrete coated with TiO_2 are widely experimented (Devahasdin et
52 al., 2003; Faraldos et al., 2016). Lasek et al. (2013) summarized the oxidation
53 mechanism, various processes and conditions of PCO for NO_x removal. Mothes et al.
54 (2018) assessed the photocatalytic performance of cement-based materials containing
55 TiO_2 for NO_x reduction, by determining the kinetic parameters under various
56 experimental conditions (relative humidity, flow rate, mixing ratio and light intensity)
57 in small-scale bed flow photoreactor experiments. Some key physic-chemical factors
58 influencing the effectiveness of photocatalytic concrete are tested in experiments by
59 (Macphee and Folli, 2016; Yang et al., 2019) on a micro level. Mendoza et al. (2017)
60 investigated the effectiveness of surface modified by WO_3/TiO_2 (WO_3, tungsten
61 trioxide) composite particles in removing gaseous NO_x under visible light irradiation.
62 Study by Guo et al. (2017) was focusing on the method of applying nano-TiO_2 to

63 concrete surface. Based on Langmuir-Hinshelwood kinetics equation, the PCO reaction
64 rate was modelled in experiments (Ballari et al., 2010). In other experiments, the
65 reaction rate was fixed considering relative humidity and irradiance (Devahasdin et al.,
66 2003; Lira et al., 2018; Yu et al., 2010).

67 In addition to concrete, experiments were also carried out on asphalt pavement (Chen
68 and Chu, 2011)(Folli et al., 2015). De Melo et al. (2012) tested road pavement overlaid
69 with cement mortar which contains varying levels of TiO_2 (3%, 6% and 10%) for their
70 photocatalytic efficiency. Results indicated that higher TiO_2 contents in a porous
71 pavement surface are more efficient in the degradation of NOx. Fan et al. (2018)
72 developed a solar photocatalytic asphalt for removing vehicular NOx and mitigating
73 roadside air pollution problem by chamber tests and field tests, who studied material
74 characterizations and evaluated the durability of the photocatalytic coating.

75 The use of TiO_2 photocatalytic nanoparticles as a road coating to trap and
76 decompose air pollutants provides a promising technology to mitigate the harmful
77 effects of vehicle emissions. Certain types of urban street layouts are known to be
78 detrimental to the dispersion of contaminants. One of the typical configurations for
79 gathering pollutants and causing harm to humans is the so-called street canyon, which
80 means a street flanked by continuous buildings on both sides. Investigations on the
81 characteristics of vehicle emissions dispersion in street canyon with TiO_2 photocatalytic
82 nanoparticles as pavement coating are very important for further understanding the
83 impact of TiO_2 photocatalytic nanoparticles pavement coating on the air quality in

84 urban environment.

85 Computational fluid dynamics (CFD) simulation is used to predict the dispersion
86 of reactive air pollutants within a street canyon, because it is quick and cost effective
87 comparing with photoreactor experiment and field measurements. Baker et al. (2004)
88 and Kikumoto and Ooka (2012) simulated the dispersion and transport of reactive air
89 pollutants (NO, NO_2 and O_3) in an urban street canyon using an LES model. Kwak et
90 al. (2013) conducted numerical simulations with a Reynolds Averaged Naviere Stokes
91 equation (RANS) model to analyze the impact of bottom heating in street canyons on
92 the flow and transport of reactive air pollutants (NO, NO_2 and O_3). Heat intensity,
93 inflow wind and vegetation were found important factors that effect on reactive
94 pollution dispersion in urban street canyon (Xie and Zhu, 2018) (Moradpour et al.,
95 2017). CFD techniques are effective tools for the simulation of reactive flow within
96 photocatalytic devices considering all the coupled phenomena taking place (Lira et al.,
97 2018). CFD has been used to model flat plate photo reactor (Passalía et al., 2011)
98 (Salvado, 2007) (Salvado and Hargreaves, 2007), multi-tube reactor (Jelle Roegiers,
99 2018) (Alpert et al., 2010), impeller reactor (Tokode et al., 2017) and rectangular reactor
100 (Einaga et al., 2015). The effects of film thickness (Vezzoli et al., 2013) and gas flow
101 rate (Alpert et al., 2010) (Einaga et al., 2015) have also been investigated. However,
102 there are few studies on CFD simulations of the effect of NOx photocatalytic oxidation
103 in street canyon with TiO_2 photocatalytic nanoparticles as pavement coating.

104 This paper aims to develop a coupled CFD-PCO model and investigate the effects of

105 TiO_2-based photocatalytic road coating on the NOx reduction in urban street canyon.
106 Furthermore, a comprehensive analysis of the key factors influencing the effectiveness
107 of the TiO_2-based photocatalytic coating road is carried out. Methodology in this study
108 will provide a fast and effective way for the investigation of the PCO reaction in street
109 canyon with TiO_2 coating road. Findings from this study shall be useful to road design
110 and transport planning to reduce reactive pollutant levels in urban traffic environment.

111 2. Methodology

112 2.1 Flow modeling

113 Computational fluid dynamics (CFD) modelling is based on numerical solutions to
114 derive dispersion equations and fluid flow simulation. These solutions are derived from
115 the principles of conservation and transmission. The air in street canyons can be
116 considered incompressible turbulent inert flow, and the density of air and pollutant is
117 assumed to be constant. As Sini et al. (1996) pointed out, these assumptions are
118 reasonable for most low-level atmospheric environments.

119 Steady RANS model has been widely used because its effectiveness in predicting
120 average airflows. Re-normalization group (RNG) $k-\varepsilon$ model is used in this study
121 according to previous research on the influence of structures on particulate matter
122 dispersion in street canyons by CFD modeling (Hao et al. 2019).

123 The commercial CFD software Fluent (Fluent, 2009) is used to implement the
124 mathematical model above. Meanwhile, the governing equations are discretized using

125 the finite volume method and the second order upwind scheme. The SIMPLE scheme
126 is used for the pressure and velocity coupling.
127 The inlet flow velocity is:
128 $$u(z) = U_0(\frac{y - H}{Y})^{\alpha} \quad (1)$$
129 where U_0 is the wind speed at the boundary, it is set as $U_0 = 3$ m-s^{-1}. H is the height
130 of the building and Y is the thickness of the boundary which is set to 80 m in the paper.
131 The same thickness was also applied in Ai and Mak's simulation (Ai and Mak, 2017).
132 α is the wind profile exponent indicating the base surface roughness in relation to the
133 terrain category of mid-dense urban area, and was set to 0.22 (Hang et al., 2017).
134 Simulations in this study are performed with a full-scaled model. Fig.1 shows the
135 computational domain. The buildings' height H and street's width W are all 20 m. The
136 ratio H/W = 1. Pollution inlet is set in the middle of the ground with 1 m wide. The
137 domain size is 20 m by 100 m in x and y directions. Regular grids of 0.1 m by 0.1 m
138 are applied to the whole area inside the street canyon. Grid size outside the canyon
139 increases as they have less effect. Velocity-inlet is applied to the air inlet. The outlet is
140 set with outflow condition. The top domain is considered symmetrical. Walls are
141 defined as non-slip walls. Temperature is set as 298K (about 25ºC) in the domain and
142 at all the walls, which means the canyons are isothermal.

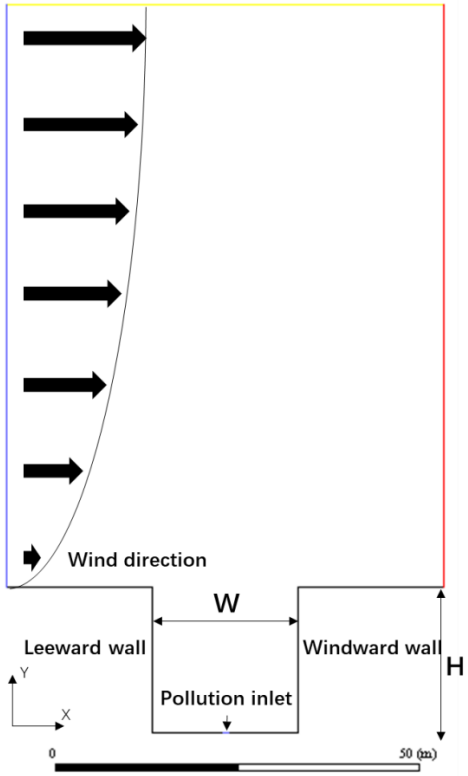

Fig.1. Computational domain

2.2 PCO reaction mechanism

A simplified photochemical steady state (PSS) O_3/NO_x model is implemented if the road is without TiO2 coating. The chemical reactions considered are (Baik et al., 2007; Carpenter et al., 1998)

$$NO_2 \xrightarrow{h\nu} NO + O^*, \quad R_1 = k_1 C_{NO_2} \tag{2}$$

$$O^* + O_2 + M \longrightarrow O_3 + M, \quad R_2 = k_2 C_{O^*} C_{O_2} C_M \tag{3}$$

$$O_3 + NO \longrightarrow NO_2 + O_2, \quad R_3 = k_3 C_{O_3} C_{NO} \tag{4}$$

In Eq.(2), $h\nu$ represents photovoltaic processes triggered by sunlight. In Eq. (3), M means a third-body molecule that absorbs energy and stabilizes O_3. Above reaction mechanism has been widely used in previous studies (García-yee et al., 2018; Han et

155 al., 2018; Muilwijk et al., 2016; Ryerson et al., 2000; Xie and Zhu, 2018).

156 The rate of Eq. (2) is considered infinitely fast compared to the photolysis rate R_1 ,

157 e.g. $k_2 \approx \infty$ (Muilwijk et al., 2016). k_1 is specified as 0.0081 s^{-1} and

158 $k_3 = 44.05 \times 10^{-3} exp(-1370/T)\, ppb^{-1} s^{-1}$ (Baik et al., 2007; Seinfeld, 2007). Eq. 2-4 are

159 combined with the steady RANS method to simulate the dispersion of NO and NO_2.

160 In this simulation, NO and NO_2 are released from the pollution inlet (Fig.1) with a

161 mole fraction of 50 ppm and 5 ppm, respectively. The releasing speed is defined as

162 0.002m/s. It corresponds to about 1000 vehicles per hour, the emission intensity of NO

163 and NO_2 are 120.7 $\mu g\, m^{-1} s^{-1}$ and 18.5 $\mu g\, m^{-1} s^{-1}$, respectively, assuming the NO_x

164 emission rate is 0.5 $g\, km/s$ per vehicle (Baker et al., 2004).

165 Furthermore, road with nanometer TiO2 coating is associated with the photocatalytic

166 oxidation (PCO) of nitrogen oxides in street canyon. The related reactions are written

167 below (Allen et al., 2003):

168 $$TiO_2 + h\nu \longrightarrow TiO_2(e^- + h^+) \quad (5)$$

169 $$O_2 + e^- \longrightarrow O_2^{\cdot -} \quad (6)$$

170 $$H_2O + h^+ \longrightarrow H^+ + HO^{\cdot} \quad (7)$$

171 $$NO + HO^{\cdot} \longrightarrow HNO_2 \quad (8)$$

172 $$HNO_2 + HO^{\cdot} \longrightarrow NO_2 + H_2O \quad (9)$$

173 $$NO_2 + HO^{\cdot} \longrightarrow NO_3^- + H^+ \quad (10)$$

174 The Langmuir-Hinshelwood model has been widely used to model the reaction rate

175 for PCO (M. M. Ballari et al., 2010; Mills and Hunte, 1997; Muñoz et al., 2019). Ballari

et al. (2010) developed equations to calculate the reaction rate of NO and NO_2 for surface reactions at constant *RH* and irradiance. Lira et al. (2018) took the effects of *RH* and irradiance into account in developing the equations, which are written below:

$$r_{NO} = -\frac{k'_{NO} C_{NO}}{1 + K_{NO} C_{NO} + K_{NO_2} C_{NO_2} + K_w C_w} (-1 + \sqrt{1 + \alpha E}) \quad (11)$$

$$r_{NO_2} = -\frac{k'_{NO_2} C_{NO_2} - k'_{NO} C_{NO}}{1 + K_{NO} C_{NO} + K_{NO_2} C_{NO_2} + K_w C_w} (-1 + \sqrt{1 + \alpha E}) \quad (12)$$

where k'_i and K_i are intrinsic kinetic and equilibrium parameters, respectively. α is kinetic parameter related to irradiance and *E* is irradiance. The constants derived by Lira et al. (2018) are based on the values derived by Ballari et al. (2010), which are taken as reference values in this study. The values are listed in Table 2.

Table 2 Values adopted in Eq. (11-12) (Lira et al., 2018)

Parameter	Value	Unit
k'_{NO}	4.18	$m \cdot s^{-1}$
k'_{NO_2}	6.73	$m \cdot s^{-1}$
K_{NO}	8.48×10^8	$m^3 \cdot kmol^{-1}$
K_{NO_2}	3.02×10^8	$m^3 \cdot kmol^{-1}$
K_w	5.07×10^4	$m^3 \cdot kmol^{-1}$
α	2.37×10^{-3}	$m^2 \cdot W^{-1}$

Photoactive components of photocatalytic coatings are activated by ultraviolet (UV) light (de Melo and Trichês, 2012)(Guo et al., 2017)(Diamanti et al., 2013). The proportion of UV light to total radiation intensity is about 8.7% (Zhang, 2014).

According to the radiation intensity and *RH* data in different region of China (National Bureau of Statistics of China, 2019), irradiance (*E*) varies in the range of 10-40 $W \cdot m^{-2}$, *RH* varies in the range of 10%-90%. *E* of 40 $W \cdot m^{-2}$ and *RH* of 50% are set as the reference condition in this study.

2.3 Calculation for pollutant conversion

In order to evaluate the effects of TiO_2 coating on the PCO reactions in street canyon, pollutant conversion (X_{NO}) is defined as:

$$X_i = \left(\frac{C_i^{noPCO} - C_i^{PCO}}{C_i^{noPCO}} \right) \times 100\% \quad (13)$$

i stands for the type of the pollutant, here refer to NO and NO_2. C_i^{PCO} means the average pollutant concentration using the model with PCO reactions. C_i^{noPCO} means the average pollutant concentration using the model without PCO reactions. The higher the X_i, the more effective the PCO reaction is.

3. Model validation

The accuracy of the above developed CFD model was evaluated using results from the wind-tunnel experiments by Allegrini et al. (2014). The validation setups for flow modeling have been detailed in previous publication (Hao et al., 2019). In order to validate the chemical reaction model, a 2D computational domain (Fig.2) with a length (*L*+*L*') of 0.4 m and a height (*H*) of 3 mm was built similar to Lira et al.'s study (Lira et al., 2018) for comparing with Ballari et al.'s experiment (M. M. Ballari et al., 2010).

The domain's height uses value 2H and 4H (keeping the length constant). The bottom of the domain with length L (0 < x < 0.2 m) is set as a reactive surface. The reaction mechanism is written in Eq. (5-10). Domain with length L' (0 < x < 0.2 m) is set as a control group without PCO to obtain a fully developed laminar velocity profile at x=0. Inlet velocity is set to 0.1667 m/s. A concentration of $4.47\times10^{-8} kmol\cdot m^{-3}$ for NO and a relative humidity of 50% is set at the inlet. A homogeneous irradiance of 10 $W\cdot m^{-2}$ is imposed at the reactive surface. Simulation results are compared to those from Lira et al.'s (Lira et al., 2018) and Ballari et al.'s experiment (M. M. Ballari et al., 2010). In order to compare the experiment results between different tests, the NO conversion (X_{NO}) is specified as:

$$X_{NO} = \left(\frac{C_{NO}^{in} - C_{NO}^{avg,out}}{C_{NO}^{in}} \right) \times 100\% \quad (14)$$

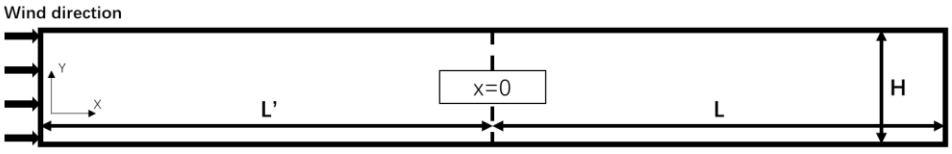

Fig.2. Computational domain for chemical reaction validation

The results including comparison with those by Lira et al. (Lira et al., 2018) are shown in Fig.3. Fig.3(a) shows the reaction rates for NO along x-axis at the reactive surface. A gap was observed when comparing the results with Lira et al.'s. However, the tendency is the same that the rates decrease along the direction of wind. The reaction rates obtained in this study are lower than in the reference study. As a result, the profiles of NO mass fractions obtained for 0<x<L (Fig.3(c)) in this study are higher than Lira et al.'s. The results for NO_2 are shown in Fig.3(b) & (d). Reaction rates of NO_2 at the

228 reactive surface show high similarity with the reference. Values of NO_2 mass fractions
229 are higher in this study, compared to the reference.
230 Results for X_{NO} in this validation comparing with reference simulation (Lira et al.,
231 2018) and experiment (M. M. Ballari et al., 2010) are shown in Fig.4. Clearly, there is
232 a tendency of decreasing X_{NO} as the relative humidity increases. It is worth noting that
233 simulation in this validation matches Ballari et al.'s experiment better than Lira et
234 al.'s study (Lira et al., 2018), although it overestimates NO conversion. After validation,
235 the chemical mechanism model applied in this study is considered reliable for
236 predicting the chemical reaction and transformation.

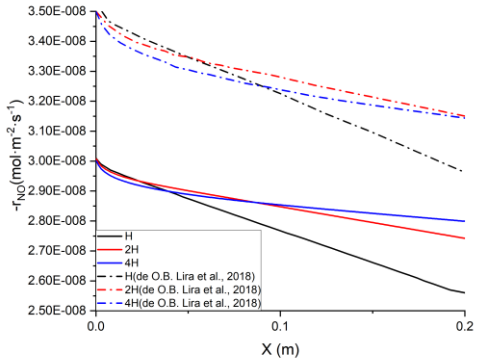

(a) Reaction rates for NO along x-axis at the reactive surface.

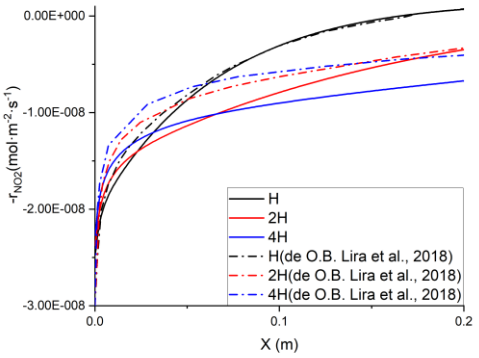

(b) Reaction rates for NO_2 along x-axis at the reactive surface.

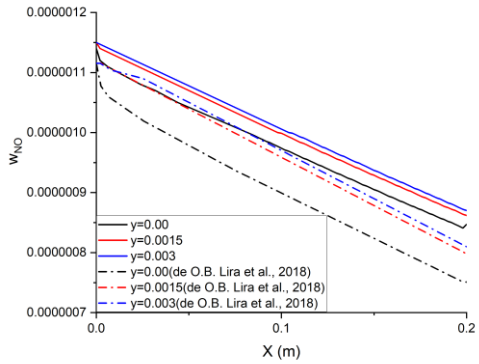

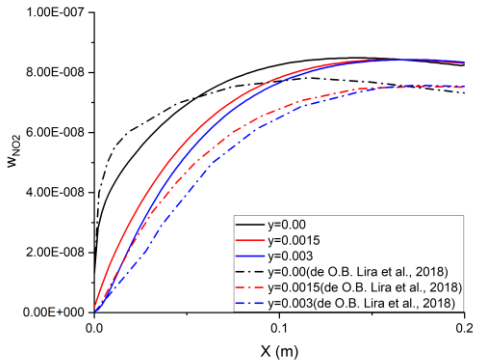

(c) Profiles of NO mass fractions obtained for 0<x<L at y= 0.00, 0.0015 and 0.003 m

(d) Profiles of NO_2 mass fractions obtained for 0<x<L at y= 0.00, 0.0015 and 0.003 m

Fig.3. Comparison results with Lira et al.

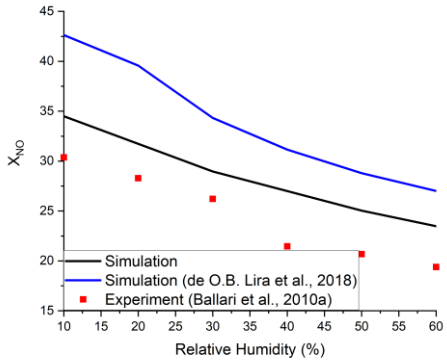

Fig.4. Comparison of NO conversion (X_{NO}) with experiment as a function of relative humidity

4. Results and discussion

4.1 NO_x dispersion in street canyon with TiO_2 coating road

In this section, simulation results of a street canyon with TiO_2 coating road are compared with a street canyon without TiO_2 coating road.

Fig.5 illustrates the wind flow structures and pollutant dispersion patterns in the street canyons with and without TiO_2 coating road. Due to the presence of clockwise eddy, most of the pollutants accumulated in the leeward side, as shown in Fig.5a and Fig.5b. Decreases of NO concentration were observed in the street canyon with TiO_2 coating road. In details, the average concentration of NO inside the street canyon with TiO_2

246 coating road is 6.06 ppm, while it is 6.29 ppm inside the street canyon without TiO_2

247 coating road, as shown in Fig.5c and Fig.5d. This means the average NO concentration

248 decreases by 3.70% under the influence of PCO reactions. Similar reduction in NO_2

249 concentration inside the canyon is shown in Fig.5e and Fig.5f. The PCO decreases the

250 average concentration of NO_2 by 4.31%.

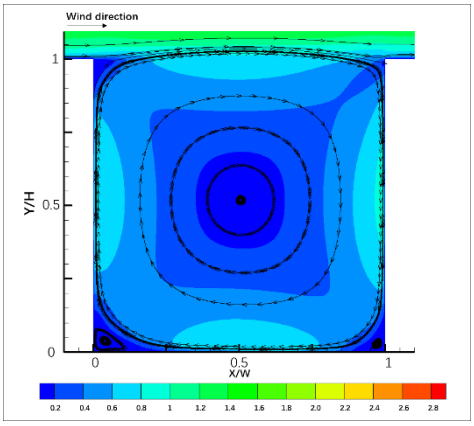

(a) Flow filed and velocity contour in canyon without TiO_2 coating road.

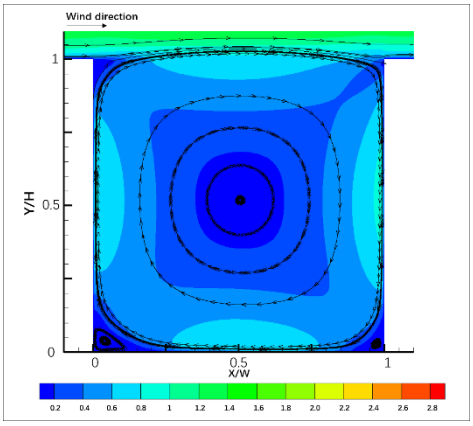

(b) Flow filed and velocity contour in canyon with TiO_2 coating road.

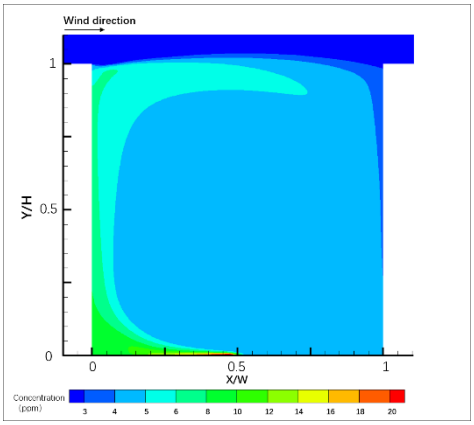

(c) Contour of NO concentration in canyon without TiO_2 coating road.

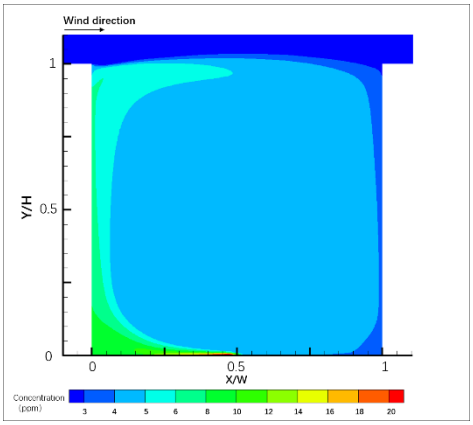

(d) Contour of NO concentration in canyon with TiO_2 coating road.

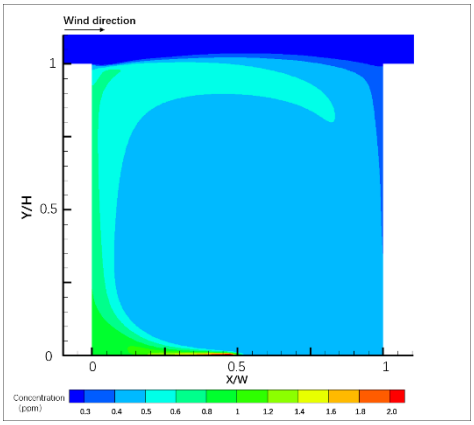

(e) Contour of NO_2 concentration in canyon without TiO_2 coating road.

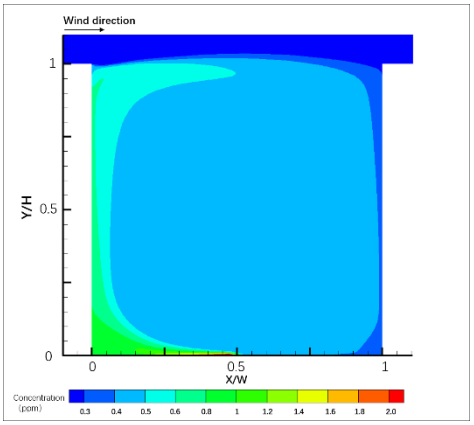

(f) Contour of NO_2 concentration in canyon with TiO_2 coating road.

Fig.5 Flow fields, contours of flow velocity and NO_x concentration in the observed street canyons.

Profiles of NO and NO_2 concentration at the leeward wall, windward wall and the breathing zone are shown in Fig.6. The breathing zone is defined as a height of y=1.5 m because it is about the nose height of the pedestrians. Concentrations at leeward and windward wall can influence the health of people who live or work in the buildings on either side of the street. It is obvious that the NOx concentration is lower in street canyons with TiO_2 coating road in all observed profiles. The average NO and NO_2 concentration at the height of breathing zone decrease by 3.29% and 3.88%, respectively, under the influence of PCO reactions. The average NO concentration near the windward wall and leeward wall decrease by 3.28% and 3.35%, respectively. The average NO_2 concentration near the windward wall and leeward wall decrease by 3.84% and 3.95%, respectively. Conclusions can thus be drawn that the PCO reactions with TiO_2 coating decrease the NO_X concentration inside street canyon. However, the characteristics of pollutant profiles are similar for street canyons with and without TiO_2

coating road. NO and NO_2 concentrations at windward wall reach high level at 0.25H<y<0.75H. Conversely, NO and NO_2 concentrations at leeward wall at 0.25H<y<0.75H are at a low level, while reaching the peak value at about y=0.05H. NO and NO_2 concentrations at breathing zone have the peak value near leeward wall (x<~0.2W). That means pedestrians near the leeward side are exposed to more pollution than at the windward side. PCO reaction with TiO_2 coating can lead to 3-4% reduction of NO and NO_2 in this area.

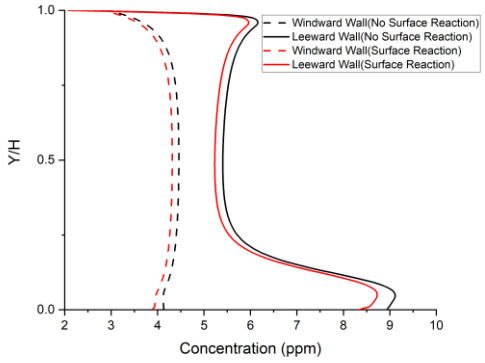

(a) Profiles of NO concentration at leeward and windward wall along 0<y<H

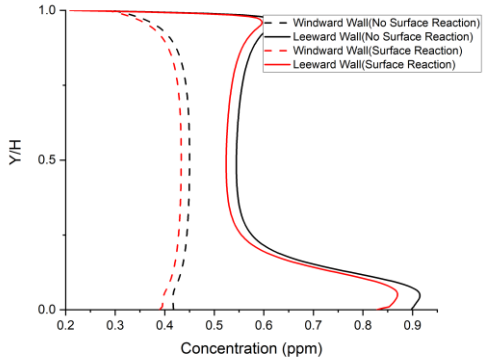

(b) Profiles of NO_2 concentration at leeward and windward wall along 0<y<H

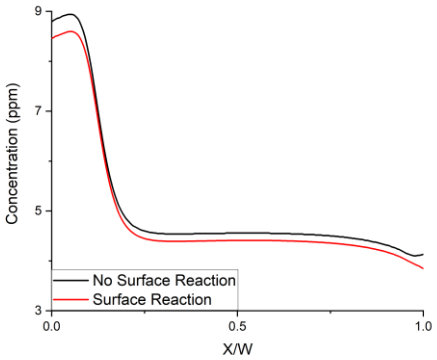

(c) Profiles of NO concentration at the breathing zone along 0<x<W

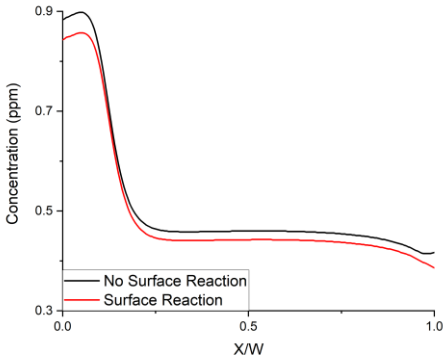

(d) Profiles of NO_2 concentration at the breathing zone along 0<x<W

Fig.6 Profiles of NO and NO2 concentration.

4.2 Effects of irradiance on PCO and NO_x profiles

Irradiance (*E*) is varied in the range of 10-40 $W \cdot m^{-2}$ when analysing the effects of irradiance on the PCO and NO_x profiles in street canyon. The relative humidity (50%) is kept constant. Fig.7 shows the profiles of NO and NO_2 concentration in relation to irradiance. At leeward wall, the peak value of NO_x concentration is at ~0.05H. The peak value decreases from 9.11ppm to 8.7ppm for NO, and from 0.92ppm to 0.87ppm for NO_2, when irradiance increase from 0 to $40 W \cdot m^{-2}$. The reductions of NO and NO_2 concentration are 4.5% and 5.4%, respectively. There is a sharp decrease along 0.05H<y<0.25H. The NO_x concentration near the roof of the leeward building has a small spike, reaching about 6 and 0.6 ppm for NO and NO_2, respectively. At windward wall, the concentration is in constant change and much lower than the leeward wall. In the breathing zone, the peak value of NO concentration is at about x=0.1W and ranges from 8.5~9 ppm with varied irradiance. The concentration falls rapidly along 0.1W<x<0.2W. The reaction rates of NO and NO_2 are monotonic functions of the irradiance (*E*), i.e. the increase of irradiance accelerates the reaction. NO and NO_2 concentrations in street canyon decrease when the irradiance increase.

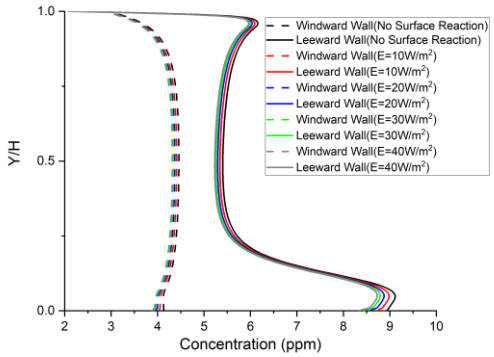

(a) Profiles of NO concentration at leeward and windward wall along 0<y<H

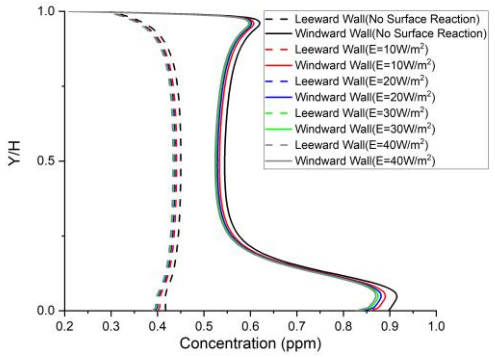

(b) Profiles of NO_2 concentration at leeward and windward wall along 0<y<H

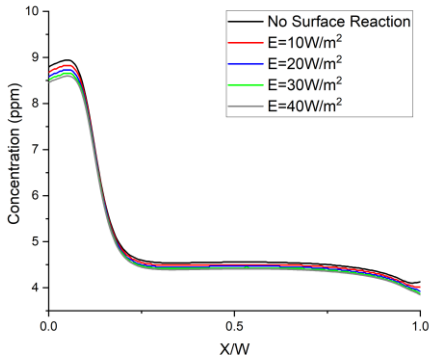

(c) Profiles of NO concentration at the breathing zone along 0<x<W

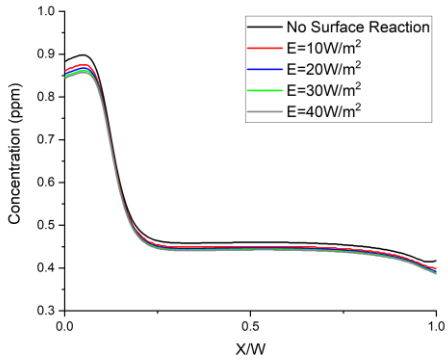

(d) Profiles of NO_2 concentration at the breathing zone along 0<x<W

Fig.7 Profiles of NO and NO2 concentration in conditions with varied irradiance.

Fig.8 presents the NO and NO_2 conversions. For both NO and NO_2, the conversion increases when the irradiance increases. The conversion at leeward wall, windward wall and breathing zone is similar. However, the average conversion of pollutants inside the whole street canyon is higher than all three zones. The PCO reaction happens on the ground while air flow still carries more pollutants to the ground and the buildings'

292 external surfaces. This explains why the NO_x is absorbed by the TiO_2 coating road but
293 the lowest NO_x conversion is not at the breathing zone which is near the ground.
294 Average conversions of NO and NO_2 in street canyon reduce from 3.70% to 1.35% and
295 from 4.31% to 2.43%, respectively, when the irradiance decreases from 40 $W \cdot m^{-2}$ to
296 $10 W \cdot m^{-2}$. It can be seen that the irradiance has a great effect on PCO reaction in a
297 street canyon with TiO_2 coating road. The higher the irradiance, the more effective the
298 PCO reaction is. The NO_2 conversion is always higher than NO, which means NO_2 is
299 more sensitive to PCO reaction in the conditions set in this study.
300

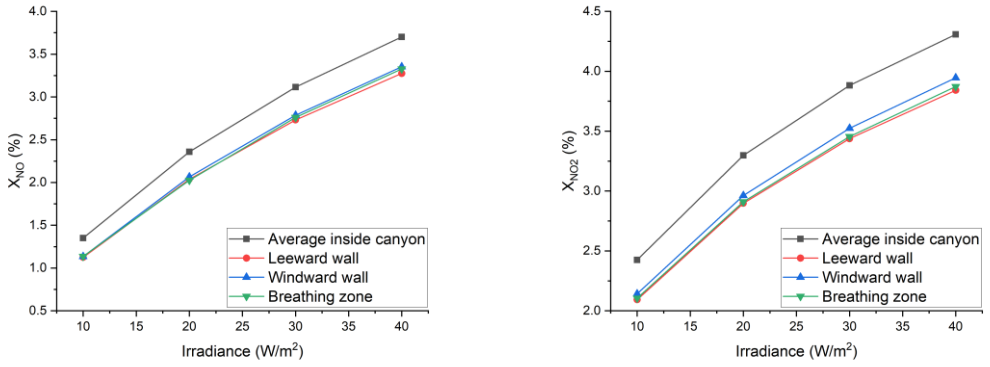

(a) NO conversion (X_{NO}) as a function of the irradiance.

(b) NO_2 conversion (X_{NO2}) as a function of the irradiance.

Fig.8 Pollutant conversion as a function of the irradiance.

301 **4.3 Effects of relative humidity on PCO and NO_x profiles**

302 The effect of relative humidity on PCO and pollutant concentration in a street canyon
303 with TiO_2 coating road is studied by changing the relative humidity (*RH*) in the range

of 10-90%. The irradiance ($40\,W\cdot m^{-2}$) is kept constant. Profiles of NO and NO_2 concentration at leeward and windward are shown in Fig.9 (a) and (b). It can be seen that the characteristics of pollutant distribution along the walls are consistent with the relative humidity. At leeward wall, the peak value of NO and NO_2 concentration is at x=~0.05H, and the maximum rising rate is 2.5% (NO) and 1.7% (NO_2) when relative humidity increases from 10% to 90%. NO and NO_2 concentration at the windward side increase more when the relative humidity increases, comparing with that at the leeward side , which see an increase of 5% (NO) and 3% (NO_2) when relative humidity increases from 10% to 90%. NO and NO_2 concentration profiles at the breathing zone is shown in Fig.9 (c)-(d). The NO and NO_2 concentration at the breathing zone rise from 2.6% to 5.3% and from 2.3% to 5.3%, respectively, when relative humidity increases from 10% to 90%. Lower relative humidity results in more effective PCO reaction and lower NO_x concentration in street canyon.

Fig.10 shows the effect of relative humidity on NO_x conversion. It is clear that when the relative humidity increases, the NO and NO_2 conversions decrease in street canyon. The same tendency can be also seen from conversions at the leeward wall, windward wall and breathing zone. However, the change rates in different locations are different. The average conversion of the whole street canyon is higher than the three zones when relative humidity is 50%-90%. The gap between the average conversion of the whole canyon and the zones gets narrower when the relative humidity decreases. When the relative humidity is 30%, the conversions of the four computational domains (whole

street cannon, leeward wall, windward wall and breathing zone) are similar. Average conversion of NO and NO_2 in street canyon decrease from 5.11% to 2.54% and from 5.60% to 3.25%, respectively, when the relative humidity increase from 10% to 90%. Within the pollutant accumulated zone, NO and NO_2 conversion at leeward wall have the greatest change with the same change of relative humidity. Along the leeward wall, the highest NO and NO_2 conversions are 5.77% and 5.23%, respectively, when *RH*=10%, and the lowest NO and NO_2 conversions are 1.17% and 1.71%, respectively, when *RH*=90%.

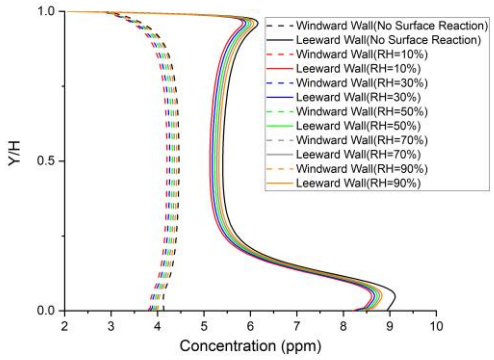

(a) Profiles of NO concentration at leeward and windward wall along 0<y<H

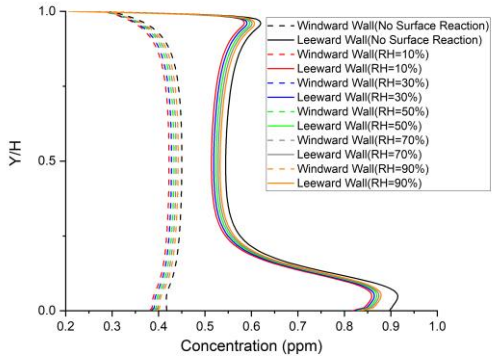

(b) Profiles of NO_2 concentration at leeward and windward wall along 0<y<H

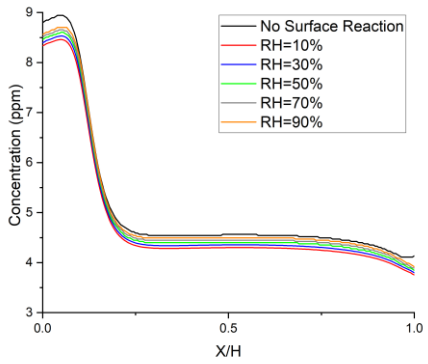

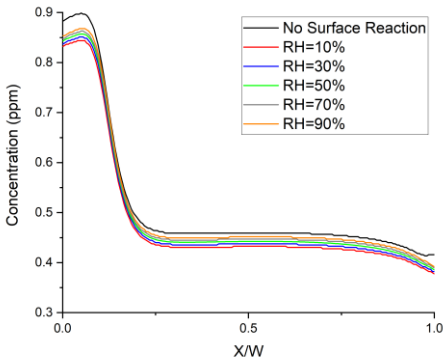

(c) Profiles of NO concentration at the breathing zone along 0<x<W

(d) Profiles of NO_2 concentration at the breathing zone along 0<x<W

Fig.9 Profiles of NO and NO2 concentration in conditions with varied relative humidity.

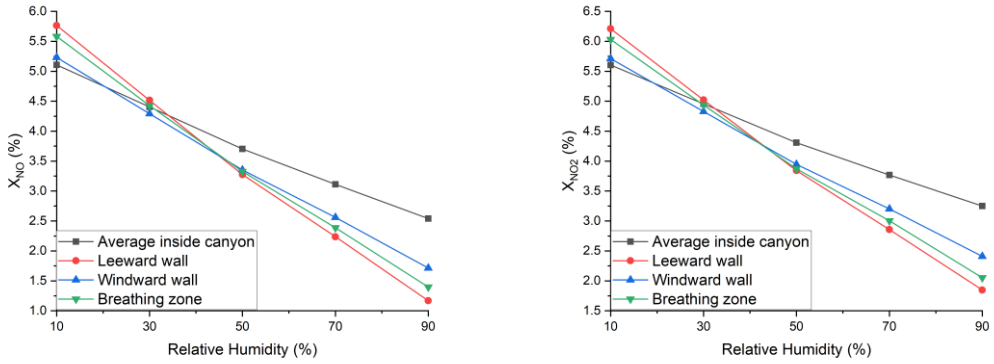

(a) NO conversion (X_{NO}) as a function of the relative humidity.

(b) NO_2 conversion (X_{NO2}) as a function of the relative humidity.

Fig.10 Pollutant conversion as a function of the relative humidity.

5. Conclusions and recommendations

A CFD model coupled with PCO reaction is implemented and validated with experimental data available in the literature for NOx abatement in a real urban street canyon with aspect ratio H/W=1. Irradiance and relative humidity are investigated, as the factors that can influence the behavior of the TiO_2 coating road with a representative TiO_2 concrete characteristic . Results show that TiO_2 coating road can effectively reduce NO_x concentration in the street canyon. The irradiance and the relative humidity have great effect on PCO reaction and on reducing the NO_x concentration in street canyon

with TiO_2 coating road. The higher the irradiance, the more effective the PCO reaction is. When the relative humidity is increased, the NO and NO_2 conversions tend to decrease.

CFD model implemented in this study can be readily used for the investigation of PCO reaction in street canyon with TiO_2 coating road. Different influencing factors can be investigated using the model, allowing for fast and effective preliminary evaluation of several scenarios aiming at the photocatalytic process. According to experiment studies (Faraldos et al., 2016; Fresno et al., 2014; Lasek et al., 2013), the behavior of TiO_2 concrete is related to the type of TiO_2 concrete and the concentration of TiO_2. For further studies, different types of TiO_2 concrete can be tested and evaluated. Other applications of TiO_2 coating may also be modeled and evaluated, for example, TiO_2 paint coated on building facades.

ACKNOWLEDGEMENTS

The work described in this paper was financially supported by National Natural Science Foundation of China (No.50808124).

References

Ai, Z.T., Mak, C.M., 2017. CFD simulation of flow in a long street canyon under a

perpendicular wind direction: Evaluation of three computational settings. Building and Environment 114, 293–306. https://doi.org/10.1016/j.buildenv.2016.12.032

Allegrini, J., Dorer, V., Carmeliet, J., 2014. Buoyant flows in street canyons: Validation of CFD simulations with wind tunnel measurements. Building and Environment 72, 63–74. https://doi.org/10.1016/j.buildenv.2013.10.021

Allen, G.., Janes, P.., Nicholson, J.., Dalton, J.., Jones, N.., Hallam, K.., 2003. Photocatalytic oxidation of NO x gases using TiO 2 : a surface spectroscopic approach. Environmental Pollution 120, 415–422. https://doi.org/10.1016/s0269-7491(02)00107-0

Alpert, S.M., Knappe, D.R.U., Ducoste, J.J., Blvd, P.P., 2010. Modeling the UV / hydrogen peroxide advanced oxidation process using computational fluid dynamics. Water Research 44, 1797–1808. https://doi.org/10.1016/j.watres.2009.12.003

Baik, J.J., Kang, Y.S., Kim, J.J., 2007. Modeling reactive pollutant dispersion in an urban street canyon. Atmospheric Environment 41, 934–949. https://doi.org/10.1016/j.atmosenv.2006.09.018

Baker, J., Walker, H.L., Cai, X., 2004. A study of the dispersion and transport of reactive pollutants in and above street canyons - A large eddy simulation. Atmospheric Environment 38, 6883–6892. https://doi.org/10.1016/j.atmosenv.2004.08.051

Ballari, Hunger, Hüsken, HBrouwers, 2010. NOx photocatalytic degradation employing concrete pavement containing titanium dioxide. Applied Catalysis B: Environmental 95, 245–254. https://doi.org/10.1016/j.apcatb.2010.01.002

Ballari, M.M., Hunger, M., Hüsken, G., Brouwers, H.J.H., 2010. Modelling and experimental study of the NO x photocatalytic degradation employing concrete pavement with titanium dioxide 151, 71–76. https://doi.org/10.1016/j.cattod.2010.03.042

Carpenter, L.J., Clemitshaw, K.C., Burgess, R.A., Penkett, S.A., Cape, J.N., McFadyen, G.G., 1998. Investigation and evaluation of the NO(x)/O 3 photochemical steady state. Atmospheric Environment 32, 3353–3365. https://doi.org/10.1016/S1352-2310(97)00416-0

Chen, M., Chu, J.W., 2011. NOxphotocatalytic degradation on active concrete road surface - From experiment to real-scale application. Journal of Cleaner Production 19, 1266–1272. https://doi.org/10.1016/j.jclepro.2011.03.001

de Melo, J.V.S., Trichês, G., 2012. Evaluation of the influence of environmental conditions on the efficiency of photocatalytic coatings in the degradation of nitrogen oxides (NOx). Building and Environment 49, 117–123. https://doi.org/10.1016/j.buildenv.2011.09.016

De Melo, J.V.S., Trichês, G., Gleize, P.J.P., Villena, J., 2012. Development and evaluation of the efficiency of photocatalytic pavement blocks in the laboratory and after one year in the field. Construction and Building Materials 37, 310–319.

https://doi.org/10.1016/j.conbuildmat.2012.07.073

Devahasdin, S., Fan, C., Li, K., Chen, D.H., 2003. TiO2photocatalytic oxidation of nitric oxide: Transient behavior and reaction kinetics. Journal of Photochemistry and Photobiology A: Chemistry 156, 161–170. https://doi.org/10.1016/S1010-6030(03)00005-4

Diamanti, M. V., Del Curto, B., Ormellese, M., Pedeferri, M.P., 2013. Photocatalytic and self-cleaning activity of colored mortars containing TiO2. Construction and Building Materials 46, 167–174. https://doi.org/10.1016/j.conbuildmat.2013.04.038

Einaga, H., Tokura, J., Teraoka, Y., Ito, K., 2015. Kinetic analysis of TiO 2 -catalyzed heterogeneous photocatalytic oxidation of ethylene using computational fluid dynamics. CHEMICAL ENGINEERING JOURNAL 263, 325–335. https://doi.org/10.1016/j.cej.2014.11.017

Fan, W., Chan, K.Y., Zhang, C., Zhang, K., Ning, Z., Leung, M.K.H., 2018. Solar photocatalytic asphalt for removal of vehicular NOx: A feasibility study. Applied Energy 225, 535–541. https://doi.org/10.1016/j.apenergy.2018.04.134

Faraldos, M., Kropp, R., Anderson, M.A., Sobolev, K., 2016. Photocatalytic hydrophobic concrete coatings to combat air pollution. Catalysis Today 259, 228–236. https://doi.org/10.1016/j.cattod.2015.07.025

Fluent, A., 2009. 12.0 Theory Guide. Ansys Inc 5.

Folli, A., Strøm, M., Madsen, T.P., Henriksen, T., Lang, J., Emenius, J., Klevebrant,

423 T., Nilsson, Å., 2015. Field study of air purifying paving elements containing
424 TiO2. Atmospheric Environment 107, 44–51.
425 https://doi.org/10.1016/j.atmosenv.2015.02.025
426 Fresno, F., Portela, R., Suárez, S., Coronado, J.M., 2014. Photocatalytic materials:
427 Recent achievements and near future trends. Journal of Materials Chemistry A 2,
428 2863–2884. https://doi.org/10.1039/c3ta13793g
429 García-yee, J.S., Torres-jardón, R., Barrera-huertas, H., Castro, T., Peralta, O., García,
430 M., 2018. Characterization of NO x -O x relationships during daytime
431 interchange of air masses over a mountain pass in the Mexico City megalopolis.
432 Atmospheric Environment 177, 100–110.
433 https://doi.org/10.1016/j.atmosenv.2017.11.017
434 Guo, M.Z., Ling, T.C., Poon, C.S., 2017. Photocatalytic NOx degradation of concrete
435 surface layers intermixed and spray-coated with nano-TiO2: Influence of
436 experimental factors. Cement and Concrete Composites 83, 279–289.
437 https://doi.org/10.1016/j.cemconcomp.2017.07.022
438 Han, B.S., Baik, J.J., Kwak, K.H., Park, S.B., 2018. Large-eddy simulation of reactive
439 pollutant exchange at the top of a street canyon. Atmospheric Environment 187,
440 381–389. https://doi.org/10.1016/j.atmosenv.2018.06.012
441 Hang, J., Luo, Z., Wang, X., He, L., Wang, B., Zhu, W., 2017. The influence of street
442 layouts and viaduct settings on daily carbon monoxide exposure and intake
443 fraction in idealized urban canyons. Environmental Pollution 220, 72–86.

https://doi.org/10.1016/j.envpol.2016.09.024

Hao, C., Xie, X., Huang, Y., Huang, Z., 2019. Study on Influence of viaduct and noise barriers on the particulate matter dispersion in street canyons by CFD Modeling. Atmospheric Pollution Research. https://doi.org/10.1016/j.apr.2019.07.003

Jelle Roegiers, 2018. CFD- and radiation field modeling of a gas phase photocatalytic multi-tube reactor. Chemical Engineering Journal 287–299.

Jiang, Q., Qi, T., Yang, T., Liu, Y., 2019. Ceramic tiles for photocatalytic removal of NO in indoor and outdoor air under visible light. Building and Environment 158, 94–103. https://doi.org/10.1016/j.buildenv.2019.05.014

Kikumoto, H., Ooka, R., 2012. A study on air pollutant dispersion with bimolecular reactions in urban street canyons using large-eddy simulations. Journal of Wind Engineering and Industrial Aerodynamics 104–106, 516–522. https://doi.org/10.1016/j.jweia.2012.03.001

Kwak, K.H., Baik, J.J., Lee, K.Y., 2013. Dispersion and photochemical evolution of reactive pollutants in street canyons. Atmospheric Environment 70, 98–107. https://doi.org/10.1016/j.atmosenv.2013.01.010

Lasek, J., Yu, Y.H., Wu, J.C.S., 2013. Removal of NOxby photocatalytic processes. Journal of Photochemistry and Photobiology C: Photochemistry Reviews 14, 29–52. https://doi.org/10.1016/j.jphotochemrev.2012.08.002

Lira, J.D.O.B., Padoin, N., Vilar, V.J.P., Soares, C., 2018. Photocatalytic NO x abatement : Mathematical modeling , CFD validation and reactor analysis.

Journal of Hazardous Materials 0–1.
https://doi.org/10.1016/j.jhazmat.2018.07.009
Macphee, D.E., Folli, A., 2016. Photocatalytic concretes — The interface between photocatalysis and cement chemistry. Cement and Concrete Research 85, 48–54. https://doi.org/10.1016/j.cemconres.2016.03.007
Mendoza, J.A., Lee, D.H., Kang, J.H., 2017. Photocatalytic removal of gaseous nitrogen oxides using WO3/TiO2 particles under visible light irradiation: Effect of surface modification. Chemosphere 182, 539–546. https://doi.org/10.1016/j.chemosphere.2017.05.069
Mills, A., Hunte, S. Le, 1997. An overview of semiconductor photocatalysis. Journal of Photochemistry and Photobiology A: Chemistry 108, 1–35. https://doi.org/10.1126/science.12.296.346-a
Moradpour, M., Afshin, H., Farhanieh, B., 2017. A numerical investigation of reactive air pollutant dispersion in urban street canyons with tree planting. Atmospheric Pollution Research 8, 253–266. https://doi.org/10.1016/j.apr.2016.09.002
Mothes, F., Ifang, S., Gallus, M., Golly, B., Boréave, A., Kurtenbach, R., Kleffmann, J., George, C., Herrmann, H., 2018. Bed flow photoreactor experiments to assess the photocatalytic nitrogen oxides abatement under simulated atmospheric conditions. Applied Catalysis B: Environmental 231, 161–172. https://doi.org/10.1016/j.apcatb.2018.03.010

Muilwijk, C., Schrijvers, P.J.C., Wuerz, S., Kenjereš, S., 2016. Simulations of photochemical smog formation in complex urban areas. Atmospheric Environment 147, 470–484. https://doi.org/10.1016/j.atmosenv.2016.10.022

Muñoz, V., Casado, C., Suárez, S., Sánchez, B., Marugán, J., 2019. Photocatalytic NOx removal: Rigorous kinetic modelling and ISO standard reactor simulation. Catalysis Today 326, 82–93. https://doi.org/10.1016/j.cattod.2018.09.001

National Bureau of Statistics of China, 2019. China Statistical Yearbook, National Bureau of Statistics of China.

National Ministry of Ecology and Environment of China, 2018. China Vehicle Environmental Management Annual Report.

Notario, A., Bravo, I., Adame, J.A., Díaz-de-Mera, Y., Aranda, A., Rodríguez, A., Rodríguez, D., 2012. Analysis of NO, NO 2, NO x, O 3 and oxidant (OX=O 3+NO 2) levels measured in a metropolitan area in the southwest of Iberian Peninsula. Atmospheric Research 104–105, 217–226. https://doi.org/10.1016/j.atmosres.2011.10.008

Passalía, C., Alfano, O.M., Brandi, R.J., 2011. Modeling and Experimental Verification of a Corrugated Plate Photocatalytic Reactor Using Computational Fluid Dynamics 9077–9086. https://doi.org/10.1021/ie200756t

Ryerson, T.B., Williams, E.J., Fehsenfeld, F.C., 2000. An efficient photolysis system for fast-response NO2measurements. Journal of Geophysical Research Atmospheres 105, 26447–26461. https://doi.org/10.1029/2000JD900389

Salvado, I., 2007. Two-Dimensional Modeling of a Flat-Plate Photocatalytic Reactor for Oxidation of Indoor Air Pollutants 7489–7496. https://doi.org/10.1021/ie070391r

Salvado, I., Hargreaves, D.M., 2007. Evaluation of the Intrinsic Photocatalytic Oxidation Kinetics of Indoor Air Pollutants 41, 2028–2035. https://doi.org/10.1021/es061569o

Seinfeld, J.H., 2007. Global Atmospheric Chemistry of Reactive Hydrocarbons. Reactive Hydrocarbons in the Atmosphere 293–319. https://doi.org/10.1016/b978-012346240-4/50009-6

Sini, J.F., Anquetin, S., Mestayer, P.G., 1996. Pollutant dispersion and thermal effects in urban street canyons. Atmospheric Environment 30, 2659–2677. https://doi.org/10.1016/1352-2310(95)00321-5

Tokode, O., Prabhu, R., Lawton, L.A., Robertson, P.K.J., 2017. Journal of Environmental Chemical Engineering A photocatalytic impeller reactor for gas phase heterogeneous photocatalysis. Journal of Environmental Chemical Engineering 5, 3942–3948. https://doi.org/10.1016/j.jece.2017.07.068

Vezzoli, M., Farrell, T., Baker, A., Psaltis, S., Martens, W.N., Bell, J.M., 2013. Optimal catalyst thickness in titanium dioxide fixed film reactors : Mathematical modelling and experimental validation. Chemical Engineering Journal 234, 57–65. https://doi.org/10.1016/j.cej.2013.08.049

Xie, X., Zhu, Z., 2018. Effects of Heat Intensity and Inflow Wind on the Reactive

528 Pollution Dispersion in Urban Street Canyon. Journal of Shanghai Jiaotong
529 University (Science) 23, 109–116. https://doi.org/10.1007/s12204-018-2030-x
530 Yang, L., Hakki, A., Zheng, L., Jones, M.R., Wang, F., Macphee, D.E., 2019.
531 Photocatalytic concrete for NOx abatement: Supported TiO2 efficiencies and
532 impacts. Cement and Concrete Research 116, 57–64.
533 https://doi.org/10.1016/j.cemconres.2018.11.002
534 Yu, Q.L., Ballari, M.M., Brouwers, H.J.H., 2010. Indoor air purification using
535 heterogeneous photocatalytic oxidation. Part II: Kinetic study. Applied Catalysis
536 B: Environmental 99, 58–65. https://doi.org/10.1016/j.apcatb.2010.05.032
537 Zhang, W., 2014. Experimental studies on automobile exhaust photocatalytic
538 degradationly Asphalt pavement Material. Chang'an University.
539 Zheng, B., Tong, D., Li, M., Liu, F., Hong, C., Geng, G., Li, H., Li, X., Peng, L., Qi,
540 J., Yan, L., Zhang, Y., Zhao, H., Zheng, Y., He, K., Zhang, Q., 2018. Trends in
541 China's anthropogenic emissions since 2010 as the consequence of clean air
542 actions. Atmospheric Chemistry and Physics 18, 14095–14111.
543 https://doi.org/10.5194/acp-18-14095-2018
544